

Tracing Andean Origins: A Machine Learning Framework for Lead Isotopes

Anibal Alviz-Meza

Grupo de Investigación en Arquitectura, Diseño e Ingeniería (GIADI), Facultad de Ingeniería y Arquitectura, Institución Universitaria Mayor de Cartagena, Cartagena, Colombia.

anibalalviz@gmail.com

Abstract: This study uses machine learning techniques to facilitate the geolocation of Andean lead isotopes, a novel approach in this geographical context. Two predictive models for latitude and longitude were developed based on the compilation of a database of the lead isotope ratios $^{206}\text{Pb}/^{204}\text{Pb}$, $^{207}\text{Pb}/^{204}\text{Pb}$, and $^{208}\text{Pb}/^{204}\text{Pb}$ from multiple Andean provinces. These models were cross-validated using GridsearchCV to assess their performance, identifying Random Forest as the best-performing model. Also, clustering analysis with the K-means model and Euclidean distance was used to correlate artifact isotope compositions with known sources. The limitations and scope of the models were listed for their appropriate usability and interpretability. This work extends basic geochronological studies, integrates a comprehensive database, and applies state-of-the-art algorithms to generate predictive models, contributing to a deeper understanding of Andean mineral resources' historical distribution and use.

Keywords: Isotopic provenance, Lead isotopes, Andes mountains, Clustering, Machine learning.

1. Introduction

This project employs machine learning techniques to boost the geo-localization accuracy of lead isotope ratios from the Andes, an approach underexplored in this geographical context. Geographic tracing of raw materials, particularly through lead isotopes, has been a well-established practice in various regions of the world, notably Europe, aiding in the historical and archaeological understanding of trade routes and cultural exchanges (Hernández-Casas, 2021). South American studies, such as those by (Craig et al., 2007) and (Parodi, 2008), have explored elemental characterization to explore the provenance of objects in the Andes, but this approach can lead to unconfident geo-localization assumptions. This limitation underscores the need for more nuanced analytical methods, as elemental analysis alone may not always yield the precise provenance of archaeological samples (Stos-Gale & Gale, 2009).

In contrast to the existing literature, lead isotope geochronological studies in the Andes have laid the groundwork for a more comprehensive understanding of regional mining practices and geological characteristics. Noteworthy studies conducted in Ecuador (Pichat et al., 2014), Chile (Puig, 1988), Argentina (Mamani et al., 2010), and Peru, covering Lake Titicaca (Guédron et al., 2021), Hualgayoc (Macfarlane, Andrew W. Petersen, 1990), Castillo de Huarmey (Tomczyk et al., 2019), Cerro de Pasco (Cooke et al., 2009), among others places, have contributed significantly to this growing database (Aitchison et al., 1995; Gunnesch et al., 1990; Kamenov et al., 2002; Kontak et al., 1990; Lechtman,

1991; Loewy et al., 2004; Macfarlane & Lechtman, 2014; Mukasa et al., 1990; Tilton & Barreiro, 1980). These works not only augment our understanding of Andean metallurgy but also offer critical data points for the development of predictive models.

Other studies developed in close contexts, based on isotopes of lead sulfur to map the provenance of archaeological remains and the classification of bioavailable strontium isotopes, both in Western Europe, have dealt with similar problems (Bataille et al., 2018, 2021). However, only the work of (Albarede et al., 2024; Rodríguez et al., 2023b) has focused on the provenance of minerals with lead isotopes, using machine learning algorithms to release a list of potential matches to explore provenance, but again focused on Europe databases. This research not only aims to consolidate a database from the Andes and generate a list of potential matches for new samples, but it also intends to provide a tool to geographically determine the possible latitude and longitude coordinates of Andes' minerals or artifacts.

Based on this, the current study aims to fill this gap by applying advanced machine learning techniques through the conformation of a large Andean isotope data set. The aim is to develop a reliable predictive tool capable of identifying the likely provenance of artifacts of suspected Andean origin. This study seeks not only to validate the effectiveness of these algorithms in a novel archaeological and geographical context but also to provide a methodology for future provenance studies in other regions. Finally, the ultimate goal is to facilitate a deeper understanding of the distribution of Andean mineral resources in South America.

2. Distribution of the Pb isotope ratios from the Andes

Pb isotope ratios are important for artifact provenance studies because the isotopic characteristics of the original metal source are maintained during artifact creation. There are four lead isotopes, ^{206}Pb , ^{207}Pb , ^{208}Pb , and ^{204}Pb ; the first three are produced by decaying uranium and thorium, while the last is not produced by radioactive decay. Thus, the isotopic composition of lead can provide information on the geographic origins of ore deposits that were historically used to manufacture archaeological artifacts. Bearing this in mind, a database was consolidated to cover a wide range of geochemical samples, including rocks, sediments, ashes, and different ores, hosting centuries of geological and human history from the Andes region. These studies are visible in Table 1.

Table 1. Studies considered for the database of Pb isotope ratios in the Andes.

Authors/year	Region	Type of samples
(Tomczyk et al., 2019)	Castillo de Huarmey, Peru	Environmental samples
(Macfarlane & Lechtman, 2014)	Peru, Bolivia, northern Chile, and northwest Argentina	Ore and mineral samples
(Pichat et al., 2014)	Chimborazo, Ecuador	Marine cores and ashes
(Mamani et al., 2010)	Peru, Bolivia, Chile, and Argentina	Igneous rocks
(Cooke et al., 2009)	Cerro de Pasco, Peru	Ores and sediment samples

(Rivera-Cornejo, 2008)	Cajamarca, Peru	Ore deposits
(Loewy et al., 2004)	Northern domain of southern Peru and northern Chile	Whole-rock samples
(Kamenov et al., 2002)	Southwest to south-central Bolivia	Ores, metal ores, crustal rocks, and leachates of crustal rocks
(Aitcheson et al., 1995)	Basement domains of the Altiplano, central Andes	Ores, volcanic rocks, and their host rocks
(Lechtman, 1991)	Central Andes/Peru	Ores
(Macfarlane, Andrew W. Petersen, 1990)	Northern Peru	Crustal rocks
(Macfarlane et al., 1990)	Central Andes	Ores and crustal rocks
(Kontak et al., 1990)	Southeastern Peru	Ore deposits
(Mukasa et al., 1990)	Central and southern Peru	Sulfide ore deposits
(Gunnesch et al., 1990)	Central Peruvian Andes	Ore and host-rock sample
(Vidal C. et al., 1990)	Central Coast of Peru	Ore deposits
(Puig, 1988)	Galenas of the Chilean Andes	Galenas
(Tilton & Barreiro, 1980)	Southern Peru	Igneous rocks

2.1 Exploration of the database of Pb isotopes

Analysis of the isotope distributions in Fig. 1 indicates that the $^{206}\text{Pb}/^{204}\text{Pb}$ and $^{208}\text{Pb}/^{204}\text{Pb}$ distributions may have a slight skewness toward the higher values, while the $^{207}\text{Pb}/^{204}\text{Pb}$ distribution appears a bit more symmetrical. All combinations show a positive correlation, although the dispersions vary. For example, the relationship between $^{207}\text{Pb}/^{204}\text{Pb}$ and $^{206}\text{Pb}/^{204}\text{Pb}$ shows a more compact clustering than the others, indicating either a more direct relationship or a shared process similarly affecting these two isotopes.

The descriptive statistic presented in Table 2 shows a remarkable variability for the $^{206}\text{Pb}/^{204}\text{Pb}$ and $^{208}\text{Pb}/^{204}\text{Pb}$ isotopes, which could be due to their greater heterogeneity among the mineral sources in the database. Likewise, the fluctuation ranges found for each isotope are considerable, despite the elimination of some outliers. On the other hand, the median is very close to the mean in all three cases, so the distribution of the isotopes is relatively symmetrical.

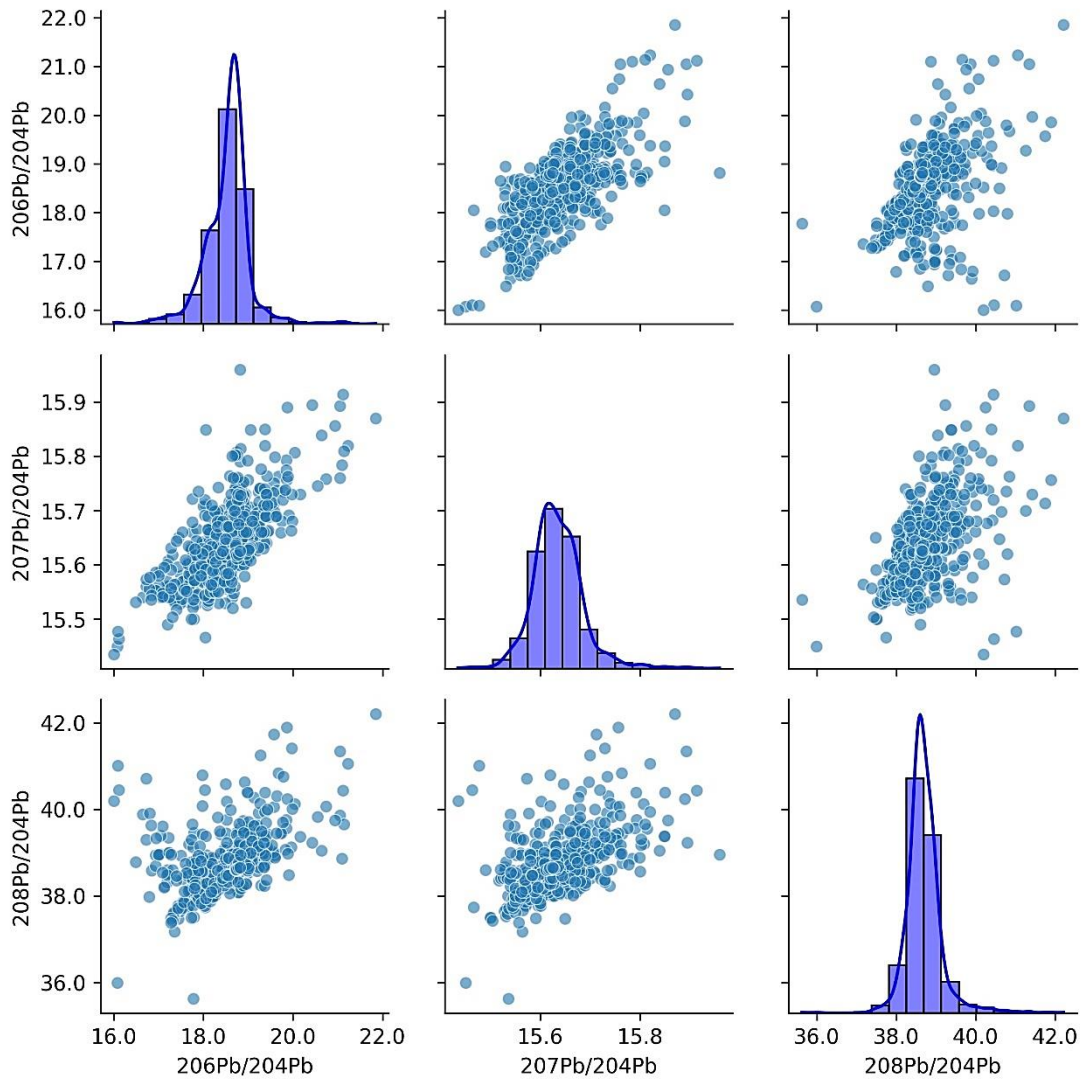


Fig. 1. Data distribution of Pb isotopes from the Andes.

Table 2. Descriptive statistic of the Pb isotope data.

	$^{206}\text{Pb}/^{204}\text{Pb}$	$^{207}\text{Pb}/^{204}\text{Pb}$	$^{208}\text{Pb}/^{204}\text{Pb}$
Count	1522	1522	1522
Mean	18.540	15.636	38.703
Std	0.512	0.052	0.467
Min	16.008	15.435	36.625
25%	18.305	15.604	38.484
50%	18.630	15.631	38.653
75%	18.780	15.663	38.879
Max	21.850	15.960	42.210

3. Clustering Analysis

The clusters obtained in this work were the result of using the unsupervised K-means model. For this, first some outliers and duplicates were eliminated, the values of the remaining isotope ratios were standardized and the elbow method was applied to select the optimal number of clusters (see Appendix A). However, the selection of the number of clusters was finally made based on the geological aspects explained at length in the work of Lechtman & Macfarlane (2014).

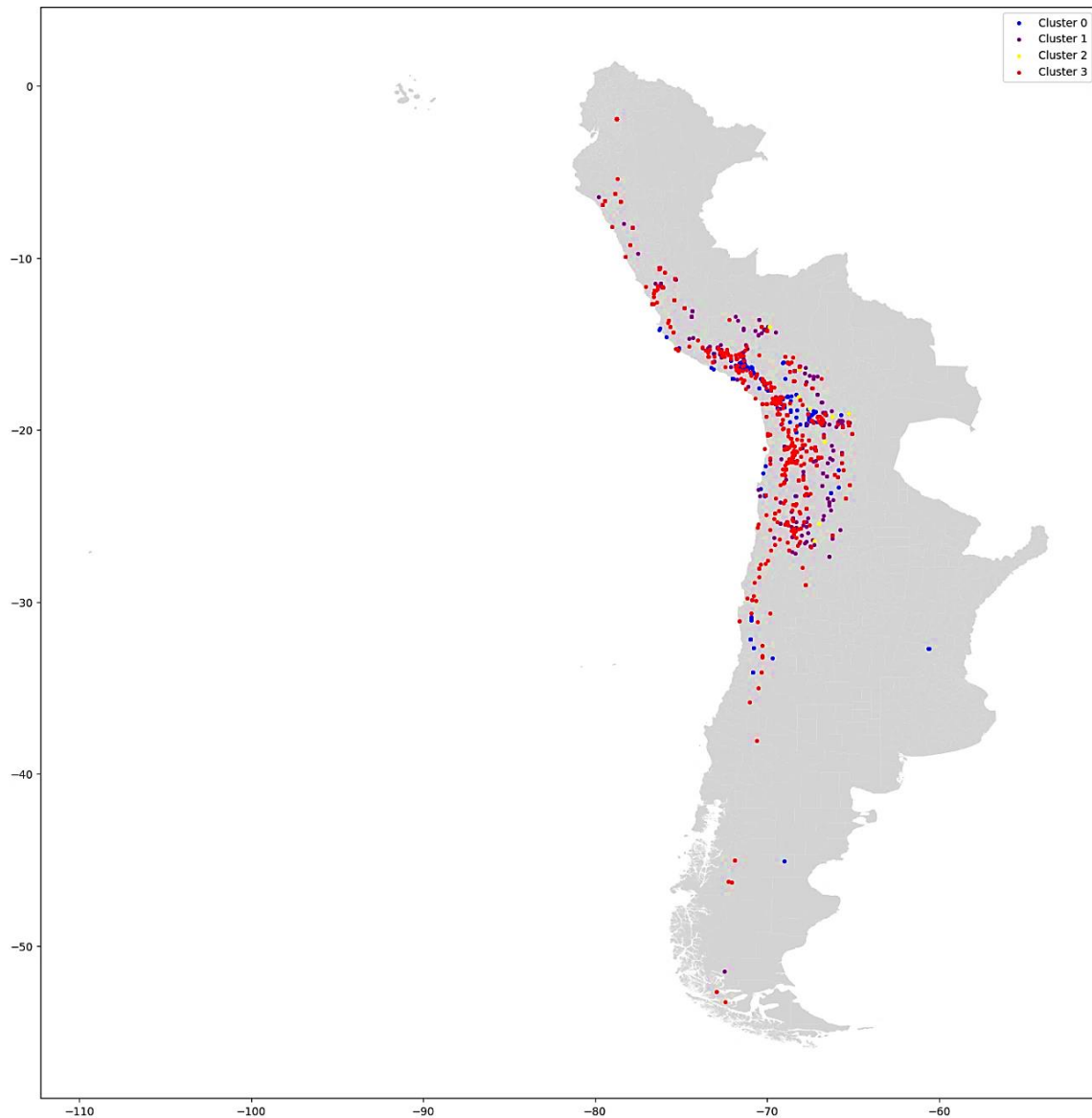


Fig. 2. Clustering of the database in 4 groups (see interactive map in supplementary material).

The lead isotope ratios corresponding to mineral deposits in the central and south-central Andes have been studied by several researchers, coinciding with the existence of 4 geographically differentiable isotope provinces (Aitchison et al., 1995; Kamenov et al., 2002; Macfarlane et al., 1990; Macfarlane & Lechtman, 2014). According to these

studies, Province I is well-adjusted to the isotope composition of orogene lead, and extends along the western margin of South America, from approximately 34° south latitude to approximately the national border between Chile and Peru. Province II is thought to be a mixing of orogenic sources in Province I and part of the upper crustal source in Province III, with locations in Peru and Chile. Province III is composed of two groups, one with higher $^{207}\text{Pb}/^{204}\text{Pb}$ and $^{208}\text{Pb}/^{204}\text{Pb}$ values than province I, whose source is the upper crust of Paleozoic sedimentary rock. While the second group of Province III resulted from mixing Province I orogenic source with a high $^{206}\text{Pb}/^{204}\text{Pb}$ upper crust. This cluster is geographically located at the rightmost of the Andes. Province IV extends from the southern coast of Peru to the western highlands and southern Bolivia, and it is characterized by having low $^{206}\text{Pb}/^{204}\text{Pb}$ and $^{207}\text{Pb}/^{204}\text{Pb}$ values compared to $^{208}\text{Pb}/^{204}\text{Pb}$ ratios. The minerals of this zone reflect mixtures between an orogenic-type source of Province I and high-grade metamorphic basement rocks.

Province I description by Lechtman & Macfarlane (2014) is coherent with the red cluster shown in Fig. 2, which in this research is extended up to Ecuador, as they originally suspected. This study shows that this cluster may cover 0° to -55° S Latitude. In Fig. 2, Lechtman & Macfarlane's Province II is included in the red cluster, in consistency with their conclusion about the orogenic source of Province II and I. The cluster blue in the same figure can be understood as an extension of Lechtman & Macfarlane's Province IV, which would initiate close to the coast of Pisco, passing through north Chile, crossing west Bolivia, and reaching Argentina. Finally, Province III is consistent with cluster yellow plus purple (see Fig. 2), which now starts from Lambayeque in Peru, crossing by west Bolivia and north Chile, to reach mainly northwest locations in Argentina.

On the other hand, in terms of Pb isotope ratios, the highest $^{207}\text{Pb}/^{204}\text{Pb}$ and $^{206}\text{Pb}/^{204}\text{Pb}$ values are related to cluster yellow while the lowest to cluster blue (see Fig. 3). In this figure, it is effectively visible that cluster purple and yellow are next together based on their $^{207}\text{Pb}/^{204}\text{Pb}$ and $^{206}\text{Pb}/^{204}\text{Pb}$ ratios. This finding is essential in the comparison of cluster purple and yellow with Lechtman & Macfarlane's Province III, which reached a similar conclusion about these ratios. Likewise, according to Fig. 4, a similar statement can be made regarding $^{208}\text{Pb}/^{204}\text{Pb}$ and $^{206}\text{Pb}/^{204}\text{Pb}$ ratios, despite the data variability, where yellow and purple cluster count with the highest values while the blue cluster with the lowest. Casually, said cluster blue, behaves similarly to Province IV described by by Lechtman & Macfarlane (2014).

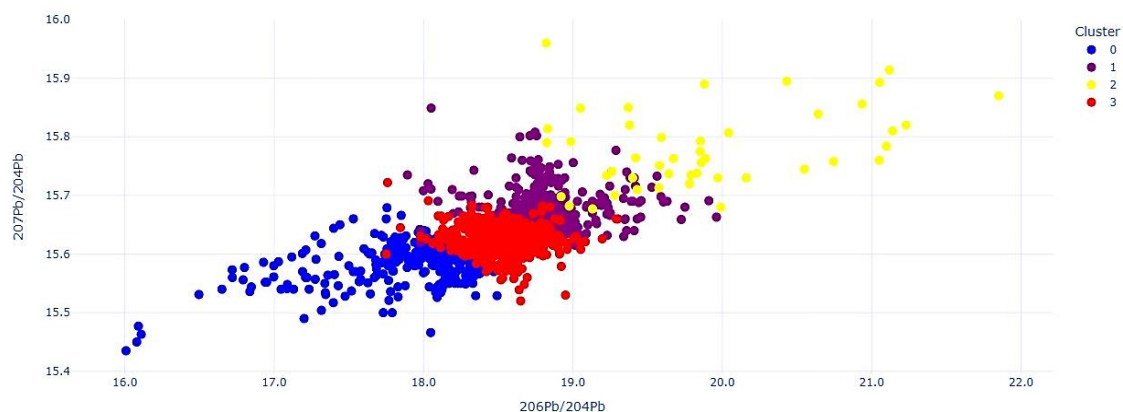


Fig. 3 . $^{207}\text{Pb}/^{204}\text{Pb}$ vs $^{206}\text{Pb}/^{204}\text{Pb}$.

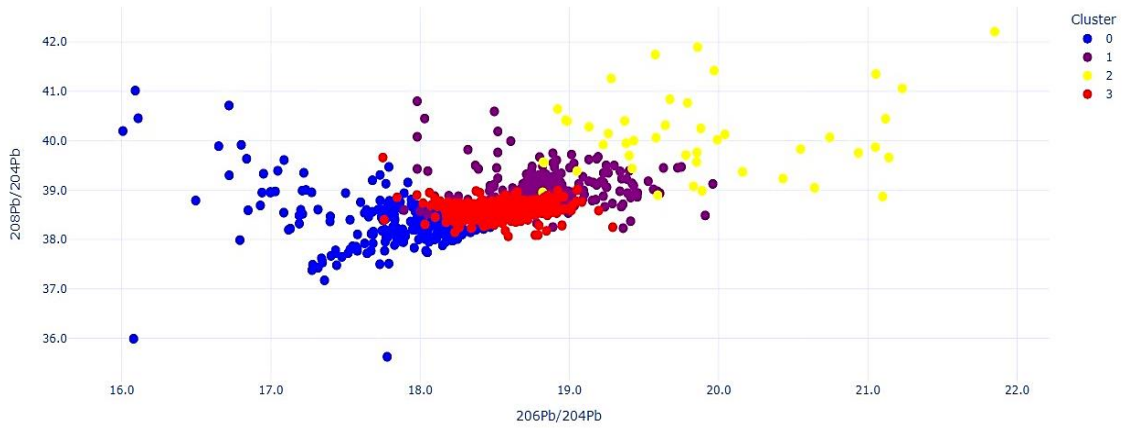


Fig. 4. $^{208}\text{Pb}/^{204}\text{Pb}$ vs $^{206}\text{Pb}/^{204}\text{Pb}$.

It is also worth mentioning that when using other unsupervised tools for clustering such as DBSCAN, the best metrics are obtained by only considering one cluster for representing the Pb isotopic signatures of the Andes.

4. Development of a Machine Learning Model for tracking of lead isotopes

Here is described step by step the procedure followed to train the Machine Learning (ML) models for the localization of artifacts, given their isotope lead signatures. Two models were developed, one to predict the coordinate Latitude based on the Pb isotope ratios $^{206}\text{pb}/^{204}\text{pb}$, $^{207}\text{pb}/^{204}\text{pb}$, and $^{208}\text{pb}/^{204}\text{pb}$. While, the second model was trained to predict the Longitude coordinate, using as well the Pb isotope ratios, but this time including the Latitude value already predicted by the first model. This general approach was selected due to the lack of homogeneous reporting in the literature revised, other than the considered three isotope lead ratios. Information about elemental composition, $^{207}\text{pb}/^{206}\text{pb}$ ratios, $^{208}\text{pb}/^{206}\text{pb}$ ratios, and other samples' isotopes could have enhanced the model's generalization capabilities. As a consequence of this approach, the Latitude coordinate led to the lowest performance by being trained only with the available pb ratios.

4.1 First Step – Data Processing

The process began with a rigorous data cleaning phase, during which outliers and duplicates were removed to ensure the quality and accuracy of the dataset, leading to 1522 examples (the same used in the cluster analysis). Subsequently, scaling was applied to the features using “StandardScaler” to normalize the ranges of the isotope data, preparing them for the ML algorithms (see Equation 1). The data set was divided into 70% for training, 20% for testing, and 10% for external validation, ensuring a reasonable evaluation of the model. A fixed seed was settled through all the experiments to maintain consistency and reproducibility of the results.

$$Z = \frac{x-\mu}{\sigma}, \text{ with } x \text{ as the original value, } \mu \text{ the media, and } \sigma \text{ the standard deviation.} \quad (1)$$

Google Colab Notebook with a CPU virtual machine of 12.7 GB RAM and 107.7 GB of disk was used to train the ML models. The experiments were performed using Python (3.10.12) and the Sklearn library (1.2.2).

4.2 Second Step – Models Training

Several ML algorithms, including SVM, KNN, Gradient Boosting, and Random Forest, were explored for both models. “GridSearchCV” was introduced for cross-validation, with a 5-iteration value to find the best hyperparameters. The cross-validation allowed for the robustness of the models and the selection of the optimal hyperparameters for each. The following hyperparameters were explored for each model:

- **KNN:** Number of neighbors: [2, 3, 4, 5, 6, 7].
- **Random Forest:** Number of estimators: [10, 50, 100, 150, 200], Maximum depth: [None, 5, 10, 20, 30, 50, 100].
- **Gradient Boosting:** Number of estimators: [50, 100, 150, 200], Learning rate: [0.001, 0.01, 0.1], Maximum depth: [3, 5, 7, 9].
- **SVM:** Kernel: ['poly', 'rbf', 'sigmoid'], Regularization parameter (C): [0.1, 1, 10, 100], Gamma: [0.001, 0.01, 0.1, 1].

K- nearest neighbors (KNN) is a simple, non-parametric algorithm used in classification (see Equation 2). It assigns a class to a sample based on the majority class among its k nearest neighbors in the feature space. The class of a sample is determined by the majority vote of its k nearest neighbors (Alviz-Meza et al., 2023). Distance metrics such as Euclidean distance are often used for this purpose.

$$Y(x) = \frac{1}{k} \sum_{i=1}^k y(i) \quad (2)$$

Where, $Y(x)$ is the prediction, k is the number of nearby neighbors, $y(i)$ are the values of the response variable for k .

Gradient Boosting is a powerful ensemble technique that builds models sequentially, each new model correcting the errors made by the previous ones, using gradient descent (Bentéjac et al., 2021). The model at stage m is shown in Equation 3:

$$Y(x) = F_0(x) + \sum_{m=1}^M \gamma_m h_m(x) \quad (3)$$

Where, $Y(x)$ is the prediction, $F_0(x)$ is the initial model, M the number of sequential trees, $h_m(x)$ is m -th decision tree prediction, and γ_m is the learning rate for the m -th tree.

Random Forest is an ensemble learning method that builds a multitude of decision trees at training time and generates the class that is the fashion of the individual tree classes (Ghalandari et al., 2023). For regression, the Random Forest output is usually the average (mean) of the predictions of all the individual trees, as expressed by Equation 4.

$$Y(x) = \frac{1}{B} \sum_{b=1}^B T_b(x) \quad (4)$$

Where, $Y(x)$ is the prediction, B the number of trees, and $T_b(x)$ is the prediction of the b -th decision tree for the input x .

Support Vector Machine (SVM) is a supervised learning model that finds the hyperplane that best separates different classes by maximizing the margin between the closest points of the classes (Liu et al., 2023). For linear SVM, the separating hyperplane is given by the equation 5.

$$w \cdot x + b = f(x) \quad (5)$$

Where w is the normal vector to the hyperplane, which target is $f(x) = 0$, and b is the bias.

On the other hand, the metrics considered for testing the performance of the models were the Mean Absolute Error (MAE), which represents the average over the test sample of the absolute differences between the prediction and the actual observation, where all individual differences have the same weight (Equation 6), the coefficient of determination (R^2), that measures how well a regression model fits the actual data (Equation 7), and the Mean Absolute Percentage Error (MAPE), which is calculated as the average unsigned percentage error, as shown in Equation 8.

$$MAE = \frac{1}{n} \sum_{i=1}^n |y_i - \hat{y}_i| \quad (6)$$

$$R^2 = 1 - \frac{\sum_{i=1}^n (y_i - \hat{y}_i)^2}{\sum_{i=1}^n (y_i - \bar{y})^2} \quad (7)$$

$$MAPE = \left(\frac{1}{n} \sum_{i=1}^n \frac{|y_i - \hat{y}_i|}{y_i} \right) \times 100\% \quad (8)$$

4.3 Third Step – Results

After analyzing the results of cross-validation with GridsearchCV for both ML models, the Random Forest model was selected as the most suitable for predicting geographic coordinates due to its superior performance metrics (see Table 2 and Table 3). In addition, the explainability of Random Forest is a crucial part of the selection, as it allows for a greater interpretation of how isotope characteristics influence geographic prediction, an aspect that is critical for acceptance and understanding in archaeological and geological investigations.

Table 2. GridsearchCV results for cross-validation to the coordinate Latitude.

	R²	MAE	MAPE	Best Params
KNN	0.30	30.86	38.34%	K = 6
Radon forest	0.45	27.63	36.87%	Max_Depth = 30 n_estimator = 200 Learning rate = 0.01
Gradient Boosting	0.44	29.44	42.52%	n_estimators = 150 Max_Depth = 7 C: 10
SVM	0.15	38.85	70.23%	Gamma: 1 Kernel: 'rbf'

Table 3. GridsearchCV results for cross-validation to the coordinate Latitude.

	R²	MAE	MAPE	Best Params
KNN	0.86	2.87	1.32	K = 6
Radon forest	0.89	2.17	1.19	Max_Depth = 50 n_estimator = 300 Learning rate = 0.1
Gradient Boosting	0.89	2.35	1.23	n_estimators = 200 Max_Depth = 5 C: 10
SVM	0.84	2.90	1.53	Gamma: 0.1 Kernel: 'rbf'

4.4 Explicability of the ML models

SHAP (SHapley Additive exPlanations), which is a method for exploring the contribution of each feature to the prediction of a model, was used to explain the models obtained. A positive SHAP value suggests that the feature increases the latitude prediction, while a negative value decreases it. Therefore, for the Latitude model, it can be easily identified that the ²⁰⁶Pb/²⁰⁴Pb ratio has the highest inclusion, positively impacting its magnitude (see Fig. 5). On the other hand, in the case of the Longitude model, Fig. 6 shows that the predicted Latitude feature has a significant negative effect, meaning that as the predicted Latitude increases, the predicted Longitude decreases. In contrast, the lead ratios indicate a smaller impact on the final values returned by the model. That is, predicted latitude is the most powerful predictor characteristic for the longitude model.

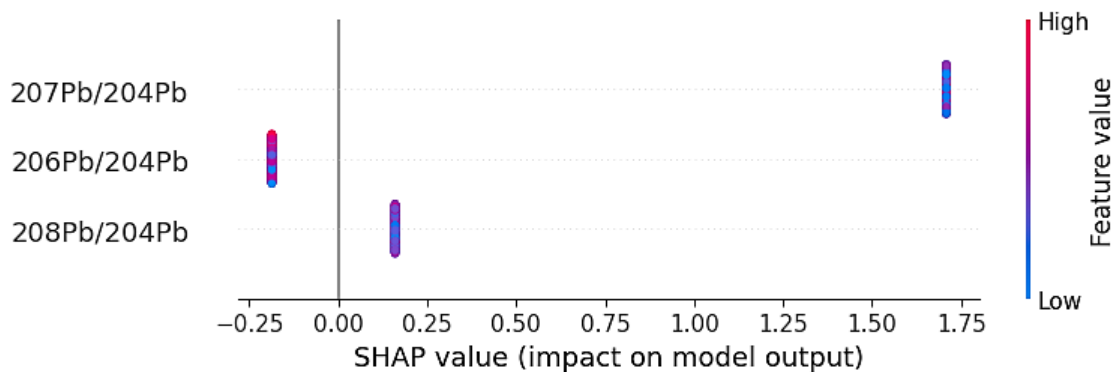


Fig. 5. SHAP for the Random Forest model for predicting Latitude.

On the other hand, for the model inference phase, some adjustment was required before deployment. For the correction of latitude and longitude predicted by the ML models, the spherical geometry of the Earth must be taken into account. Latitude is adjusted directly since the distance represented by one degree is approximately constant (111 km per degree). For longitude, the actual distance represented by each degree is fitted as a function of latitude, using the cosine of the predicted latitude. This allows an accurate representation on an interactive world map such as the Folium library (python), considering the actual geographical differences at different latitudes. This ensures that the areas of uncertainty reflect the actual geospatial variation.

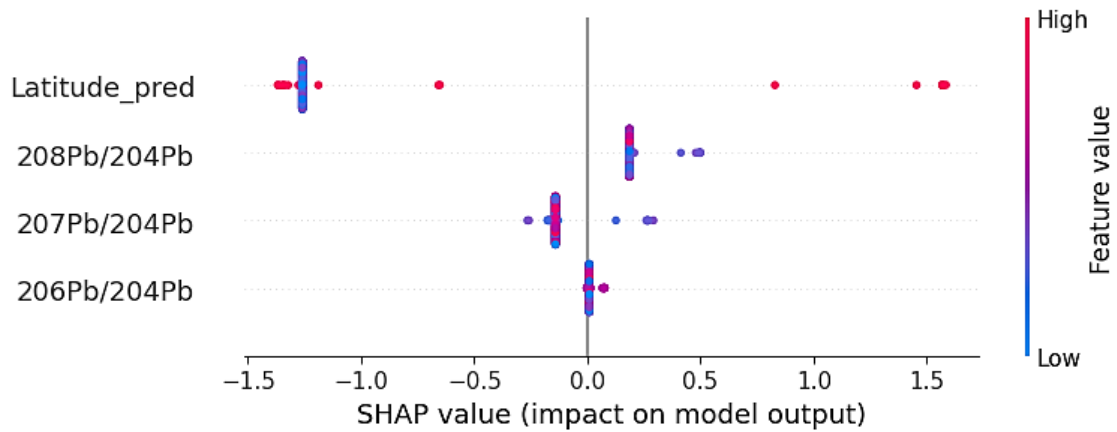


Fig. 6. SHAP for the Random Forest model for predicting Longitude.

4.5 External validation

About 150 data not previously seen by the model -randomly selected- were used to perform external validation of the ML models, obtaining very good metrics of their generalization capacity with new inputs (see Table 4). The longitude coordinate deployed a fairly high accuracy, giving a high confidence to the model in general terms. Whereas, the Latitude predictions, with their limitations, are not bad, leading to relatively reliable geographic points, as a first indication for some artifact provenience exploration.

Table 4. Metrics for both models after external validation.

	R²	MAE	MAPE
Latitude	0.94	1.30	10.13%
Longitude	0.99	0.24	0.34%

5. Euclidean distance for matching database sources

Once the ML models were developed, the next step was to develop a complementary tool to match Pb isotopes with their most similar pairs in the database. This combination enriches the analysis, not only predicting provenance but also validating and refining predictions against a consolidated dataset. Integrating both methods ensures that the obtained approach is not only based on a single methodology, making the final conclusions more robust and reliable.

Euclidean distance is used to measure the similarity between two elements, in this case, to compare the isotopic composition of archaeological artifacts with possible known sources from different mining sites (Rodríguez et al., 2023a; Stos-Gale & Gale, 2009). However, in the study of Rodríguez et al. (2023a), it is recommended to consider the uncertainty of the measurements in the database to suggest more suitable algorithms. Sadly, the approach of this work could not use said focus since the analytical uncertainty of all the articles or reports lacked that information. Therefore, it was decided to employ a conservative approach with the traditional Euclidean distance as the measure of lead isotopic comparison. This method allows for a consistent quantitative evaluation, without

considering specific variations in uncertainty. Future research may explore alternative approaches as uncertain information becomes available. Equation 9 represents the Euclidean distance used, where x represents to $^{206}\text{Pb}/^{204}\text{Pb}$, y to $^{207}\text{Pb}/^{204}\text{Pb}$, and z to $^{208}\text{Pb}/^{204}\text{Pb}$.

$$d(x, y, z) = \sqrt{(x_1 - x_2)^2 + (y_1 - y_2)^2 + (z_1 - z_2)^2} \quad (9)$$

6. Use Case

For this exercise, it was used recent data reported from silver and copper artifacts found in one intact pre-Columbian tomb of the Wari culture at Castillo de Huarmey in Peru (Kałaska et al., 2022). The authors explored the provenance of 15 objects, from which the copper sample MK 33 was randomly selected (see Table 5).

Table 5. Pb isotope ratios of the sample MK 33 from the work of Kałaska et al. (2022).

	$^{206}\text{Pb}/^{204}\text{Pb}$	$^{207}\text{Pb}/^{204}\text{Pb}$	$^{208}\text{Pb}/^{204}\text{Pb}$
MK 33	18.650	15.668	38.840

The MK 33 sample was extracted from a copper wire and is thought to be from Bolivian deposits, suggesting long-distance interactions between Castillo de Huarmey and communities such as Tiwanaku. Using the ML models pointed out a different suggestion of the sample's deposit origin (see Fig. 7). This result indicates that the Pb isotopes of the MK 33 sample are congruent with those contained in the consolidated database for that area, which should not be confused as a direct estimation of the mine of provenance, from which the ore from which the copper piece was made was extracted. To confirm the actual provenance, a careful review of the most similar lead ratios available in the database is required, so the coordinate prediction method is not sufficient on its own.

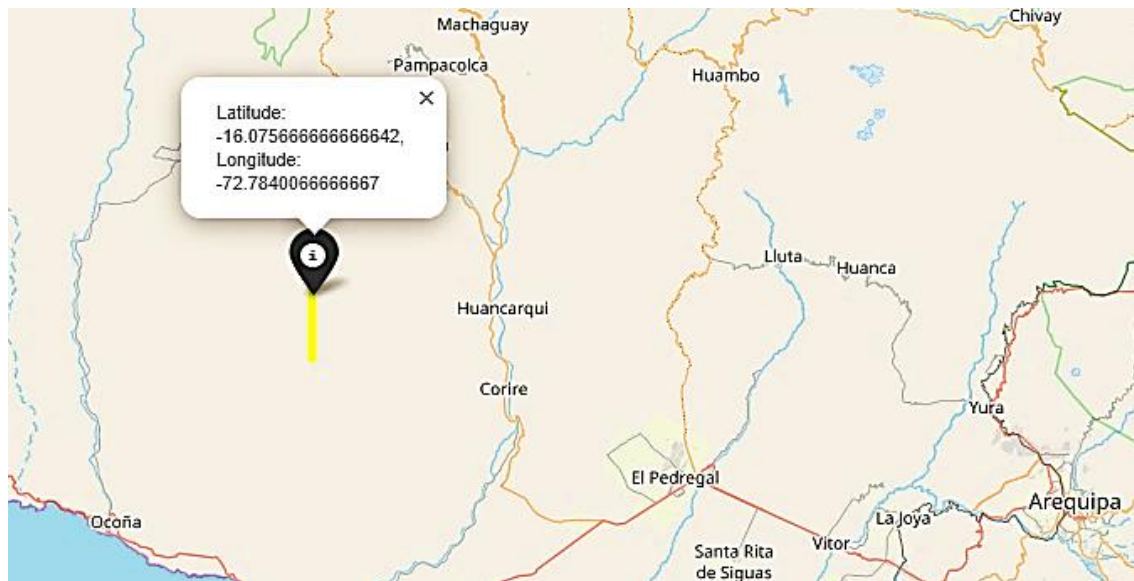


Fig. 7. Latitude and Longitude coordinates predicted for the Pb isotope ratios of sample MK 33.

Now, by pairing the Pb data from sample MK 33 with the database Pb ratios, it is used the Euclidean distance clustering expression, getting the results shown in Fig. 8. At this point, the three close matches come from three different research papers, and the lowest Euclidean distance should be prioritized. In this sense, it is found that Cotahuasi (Peru) would be the best candidate. However, before drawing any conclusions, it should be confirmed in the work of Mamani et al. (2010) and other available scientific literature whether the mineral deposits analyzed in this region were in use for the manufacture of copper artifacts at the time of the artifacts' date. In this particular case, no evidence was found that the Wari or other Andean cultures developed copper mining activities in Cotahuasi in pre-Columbian times. Thus, we move towards the next possible origin with less Euclidean distance value, which is Hualgayoc (Peru) according to Macfarlane & Petersen's (1990) study, nevertheless, it is not clear that copper was extracted from Hualgayoc in pre-Columbian times, conducting to its discarding either. Finally, Cococoro (Bolivia) is a location suggested by the copper ore samples examined by Lechtman & Macfarlane (2014). Some research work suggests that Corocoro could have been used for copper extraction in pre-Columbian times (Avila-Salinas, 1990), given the existence of multiple potential copper ores in that zone. Even more so, considering the demonstrated competence of Andean cultures in copper ore smelting techniques before the arrival of the Spanish (Caley & Easby, 1959). This final selection ends up being similar to the one reached by Kałaska et al. (2022). In any case, it is recommended to perform copper isotope analysis at Corocoro to compare with those obtained from the MK 33 sample.

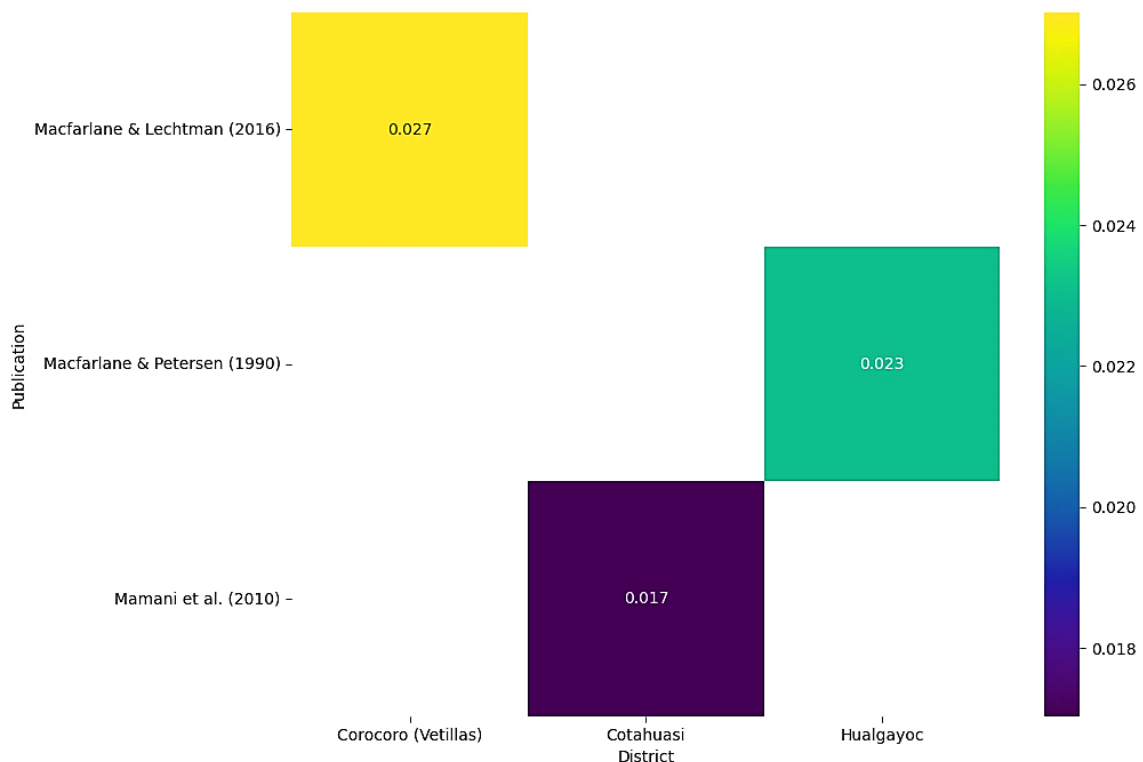


Fig. 8. Mosaic plot based on the Euclidean distance of the possible source locations of the MK 33 sample in context with the associated publications.

Given all this, it is also important to note that the coordinate predictions previously made in Fig. 7 for the MK 33 sample are consistent with the best match provided by the Euclidean distance analysis.

7. Limitations and Scope of the ML Models

Some of the identified limitations not already mentioned in the document are listed below.

- a) Geologic or anthropogenic changes over time may affect the applicability of the model for historical periods other than those represented in the training data.
- b) The training data set may not include all existing lead isotope data from the Andes.
- c) The accuracy of the model depends on the quality, completeness, and representativeness of the database used for training. Therefore, if the provenance of some artifact is tried to be determined for samples in regions not covered by the database, the model would be highly prone to errors.
- d) Objects containing lead artifacts may be manufactured from minerals from multiple sources or by re-smelting metals, complicating the assignment of a single source location.
- e) The analytical uncertainty carried over from the measurements made by the various studies and laboratories is also persistent in the obtained database.
- f) ML models require their joint operation with data matching based on Euclidean distance for reliable conclusions.
- g) The results obtained are intended to be used as a guideline that requires confirmation with additional chemical analysis and state-of-the-art reviews to get trustable conclusions.

8. Conclusions

This study demonstrates the potential of machine learning and clustering analysis to trace the provenance of archaeological artifacts through lead isotope ratios, offering a new methodological approach to historical and geological investigations in the Andes. While the models are promising, the study also recognizes limitations such as the impact of re-smelting of metals, the integrity of the dataset, the simultaneous need for using clustering and regression models, and the need for further validation. The application of these models to real archaeological sites emphasizes the importance of interdisciplinary approaches to unraveling the complex lead isotope distribution in the Andes.

9. Acknowledgments

I would like to personally thank the Universidad del País Vasco and the researcher Javier Rodríguez Aller for their invaluable support and shared experience in this scientific effort.

References

- Aitcheson, S. J., Harmon, R. S., Moorbath, S., Schneider, A., Soler, P., Soria-Escalante, E., Steele, G., Swainbank, I., & Wörner, G. (1995). Pb isotopes define basement domains of the Altiplano, Central Andes. *Geology*, *23*(6), 555–558. [https://doi.org/https://doi.org/10.1130/0091-7613\(1995\)023<0555:PIDBDO>2.3.CO;2](https://doi.org/https://doi.org/10.1130/0091-7613(1995)023<0555:PIDBDO>2.3.CO;2)
- Albarede, F., Davis, G., Blichert-Toft, J., Gentelli, L., Gitler, H., Pinto, M., & Telouk, P. (2024). A new algorithm for using Pb isotopes to determine the provenance of bullion in ancient Greek coinage. *Journal of Archaeological Science*, *163*, 105919. <https://doi.org/10.1016/J.JAS.2023.105919>
- Alviz-Meza, A., Torres-Salazar, E., Gastiaturú-Morales, S., Alvarez-Vasquez, H., Orozco-Agamez, J., & Peña-Ballesteros, D. (2023). Machine Learning Models for Natural Gas Consumer Decision Making: Case Study of a Colombian Company. *Chemical Engineering Transactions*, *100*, 169–174. <https://doi.org/10.3303/CET23100029>
- Avila-Salinas, W. (1990). Origin of the Copper Ores at Corocoro, Bolivia. *Stratabound Ore Deposits in the Andes*, 659–670. https://doi.org/10.1007/978-3-642-88282-1_52
- Bataille, C. P., Jaouen, K., Milano, S., Trost, M., Steinbrenner, S., Crubézy, É., & Colleter, R. (2021). Triple sulfur-oxygen-strontium isotopes probabilistic geographic assignment of archaeological remains using a novel sulfur isoscape of western Europe. *PLOS ONE*, *16*(5), e0250383. <https://doi.org/10.1371/JOURNAL.PONE.0250383>
- Bataille, C. P., von Holstein, I. C. C., Laffoon, J. E., Willmes, M., Liu, X. M., & Davies, G. R. (2018). A bioavailable strontium isoscape for Western Europe: A machine learning approach. *PLOS ONE*, *13*(5), e0197386. <https://doi.org/10.1371/JOURNAL.PONE.0197386>
- Bentéjac, C., Csörgő, A., & Martínez-Muñoz, G. (2021). A comparative analysis of gradient boosting algorithms. *Artificial Intelligence Review*, *54*(3), 1937–1967. <https://doi.org/10.1007/S10462-020-09896-5/METRICS>
- Caley, E. R., & Easby, D. T. (1959). The Smelting of Sulfide Ores of Copper in Preconquest Peru. *American Antiquity*, *25*(1), 59–65. <https://doi.org/10.2307/276679>
- Cooke, C. A., Wolfe, A. P., & Hobbs, W. O. (2009). Lake-sediment geochemistry reveals 1400 years of evolving extractive metallurgy at Cerro de Pasco, Peruvian Andes. *Geology*, *37*(11), 1019–1022.
- Craig, N., Speakman, R. J., Popelka-Filcoff, R. S., Glascock, M. D., Robertson, J. D., Shackley, M. S., & Aldenderfer, M. S. (2007). Comparison of XRF and PXRF for analysis of archaeological obsidian from southern Perú. *Journal of Archaeological Science*, *34*(12), 2012–2024. <https://doi.org/10.1016/j.jas.2007.01.015>
- Ghalandari, M., Mukhtar, A., Yasir, A. S. H. M., Alkhabbaz, A., Alviz-Meza, A., Cárdenas-Escrocia, Y., & Le, B. N. (2023). Thermal conductivity improvement in a green building with Nano insulations using machine learning methods. *Energy Reports*, *9*, 4781–4788. <https://doi.org/10.1016/J.EGYR.2023.03.123>

- Guédron, S., Tolu, J., Delaere, C., Sabatier, P., Barre, J., Heredia, C., Brisset, E., Campillo, S., Bindler, R., Fritz, S. C., Baker, P. A., & Amouroux, D. (2021). Reconstructing two millennia of copper and silver metallurgy in the Lake Titicaca region (Bolivia/Peru) using trace metals and lead isotopic composition. *Anthropocene*, 34. <https://doi.org/10.1016/j.ancene.2021.100288>
- Gunnesch, K. A., Baumann, A., & Gunnesch, M. (1990). Lead isotope variations across the central Peruvian Andes. *Economic Geology*, 85(7), 1384–1401. <https://doi.org/10.2113/gsecongeo.85.7.1384>
- Hernández-Casas, Y. (2021). *Investigación del metal y Arqueología Medieval en la península ibérica: estado de la cuestión y nuevas perspectivas | Arqueología y Territorio Medieval*. Arqueología y Territorio Medieval. <https://doi.org/10.17561/aytm.v28.6898>
- Kałaska, M., Mathur, R., Kamenov, G., Chyla, J., Prządka-Giersz, P., & Giersz, M. (2022). Deciphering the origin of small metal artifacts from Castillo de Huarmey (Peru) with Pb, Cu, and Ag isotopes. *Archaeometry*. <https://doi.org/10.1111/ARCM.12775>
- Kamenov, G., MacFarlane, A. W., & Riciputi, L. (2002). Sources of lead in the San Cristobal, Pulacayo, and Potosí mining districts, Bolivia, and a reevaluation of regional ore lead isotope provinces. *Economic Geology*, 97(3), 573–592. <https://doi.org/10.2113/gsecongeo.97.3.573>
- Kontak, D. J., Cumming, G. L., Krstic, D., Clark, A. H., & Farrar, E. (1990). Isotopic composition of lead in ore deposits of the Cordillera Oriental, southeastern Peru. *Economic Geology*, 85(7), 1584–1603. <https://doi.org/10.2113/gsecongeo.85.7.1584>
- Lechtman, H. (1991). The production of copper-arsenic alloys in the central Andes: Highland ores and coastal smelters? *Journal of Field Archaeology*, 18(1), 43–76. <https://doi.org/10.1179/009346991791548780>
- Liu, W., Shen, Y., Aungkulanon, P., Ghalandari, M., Le, B. N., Alviz-Meza, A., & Cárdenas-Escrocia, Y. (2023). Machine learning applications for photovoltaic system optimization in zero green energy buildings. *Energy Reports*, 9, 2787–2796. <https://doi.org/10.1016/J.EGYR.2023.01.114>
- Loewy, S. L., Connelly, J. N., & Dalziel, I. W. (2004). An orphaned basement block: The Arequipa-Antofalla Basement of the central Andean margin of South America. *Geological Society of America Bulletin*, 116(1–2), 171–187. <http://www.ajsonline.org/content/307/2/371.short>
- Macfarlane, Andrew W. Petersen, U. (1990). Pb Isotopes of the Hualgayoc Area, Northern Peru: Implications for Metal Provenance and Genesis of a Cordilleran Polymetallic Mining District. *Economic Geology*, 85, 1303–1327.
- Macfarlane, A. W., & Lechtman, H. N. (2014). Andean Ores, Bronze Artifacts, and Lead Isotopes: Constraints on Metal Sources in Their Geological Context. *Journal of Archaeological Method and Theory*, 23(1), 1–72. <https://doi.org/10.1007/s10816-014-9225-8>
- Macfarlane, A. W., Marcet, P., LeHuray, A. P., & Petersen, U. (1990). Lead isotope provinces of the Central Andes inferred from ores and crustal rocks. *Economic*

Geology, 85(8), 1857–1880.

- Mamani, M., Wörner, G., & Sempere, T. (2010). Geochemical variations in igneous rocks of the Central Andean orocline (13°S to 18°S): Tracing crustal thickening and magma generation through time and space. *GSA Bulletin*, 122(1–2), 162–182. <https://doi.org/10.1130/B26538.1>
- Mukasa, S. B., Vidal C., C. E., & Injoque-Espinoza, J. (1990). Pb isotope bearing on the metallogenesis of sulfide ore deposits in central and southern Peru. *Economic Geology*, 85(7), 1438–1446. <https://doi.org/10.2113/gsecongeo.85.7.1438>
- Parodi, L. M. V. (2008). Plateros indígenas en el Virreinato del Perú, siglos XVI y XVII. In *Buenaventura*.
- Pichat, S., Abouchami, W., & Galer, S. J. G. (2014). Lead isotopes in the Eastern Equatorial Pacific record Quaternary migration of the South Westerlies. *Earth and Planetary Science Letters*, 388, 293–305. <https://doi.org/10.1016/j.epsl.2013.11.035>
- Puig, A. (1988). Geologic and metallogenic significance of the isotopic composition of lead in galenas of the Chilean Andes. *Economic Geology*, 83(4), 843–858. <https://doi.org/10.2113/gsecongeo.83.4.843>
- Rivera-Cornejo, R. (2008). *PARTICIPACIÓN EN LOS TRABAJOS FINALES DE INTERPRETACIÓN DE ISÓTOPOS DE PLOMO DE LOS PÓRFIDOS DE ORO, COBRE Y MOLIBDENO DEL NORTE DEL PERÚ – REGIÓN CAJAMARCA*. UNIVERSIDAD DE SAO PAULO.
- Rodríguez, J., Sinner, A. G., Martínez-Chico, D., & Francisco Santos Zalduegui, J. F. (2023a). AMALIA, A Matching Algorithm for Lead Isotope Analyses: Formulation and proof of concept at the Roman foundry of Fuente Spitz (Jaén, Spain). *Journal of Archaeological Science: Reports*, 51(August). <https://doi.org/10.1016/j.jasrep.2023.104192>
- Stos-Gale, Z. A., & Gale, N. H. (2009). Metal provenancing using isotopes and the Oxford Archaeological lead isotope database (OXALID). *Archaeological and Anthropological Sciences*, 1(3), 195–213. <https://doi.org/10.1007/S12520-009-0011-6/TABLES/7>
- Tilton, G. R., & Barreiro, B. A. (1980). Origin of lead in Andean calc-alkaline lavas, Southern Peru. *Science*, 210(4475), 1245–1247. <https://doi.org/10.1126/science.210.4475.1245>
- Tomczyk, W., Giersz, M., Sołtysiak, A., Kamenov, G., & Krigbaum, J. (2019). Patterns of camelid management in Wari Empire reconstructed using multiple stable isotope analysis: evidence from Castillo de Huarmey, northern coast of Peru. *Archaeological and Anthropological Sciences*, 11(4), 1307–1324. <https://doi.org/10.1007/s12520-017-0590-6>
- Vidal C., C. E., Injoque-Espinoza, J., Sidder, G. B., & Mukasa, S. B. (1990). Amphibolitic Cu-Fe skarn deposits in the central coast of Peru. *Economic Geology*, 85(7), 1447–1461. <https://doi.org/10.2113/gsecongeo.85.7.1447>

Appendix A

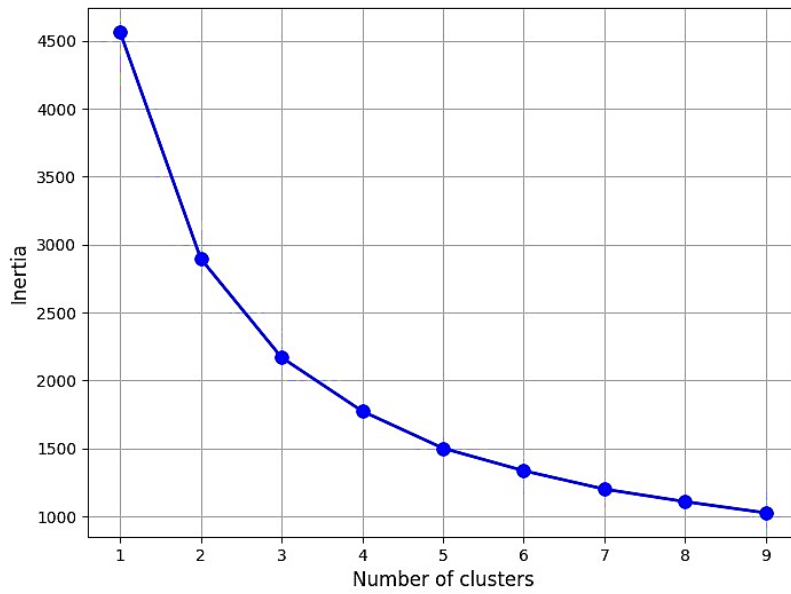


Fig. A1. Elbow plot for k-means optimization.

Table A1. Clusters metrics and conformation.

	Performance	Agrupation
2 Clusters	0.37	$C_0= 694, C_1= 828$
3 Clusters	0.38	$C_0= 619, C_1= 824, C_2= 79$
4 Clusters	0.32	$C_0= 326, C_1= 486, C_2= 45,$ $C_3 = 665$
5 Clusters	0.33	$C_0= 340, C_1= 455, C_2= 44,$ $C_3 = 33, C_4= 650$